First-principles study of the structural, electronic, and elastic properties of $R\mathrm{Rh_3B}_x\mathrm{C}_{1-x}$ (R=Sc and Y)

Ryoji Sahara,* Toetsu Shishido, and Akiko Nomura
Institute for Materials Research, Tohoku University, Aoba-ku, Sendai 980-8577, Japan

Kunio Kudou
Faculty of Engineering, Kanagawa University, 3-27-1 Rokkakubashi, Kanagawa-ku, Yokohama 221-8686, Japan

Shigeru Okada
Faculty of Engineering, Kokushikan University, 4-28-1 Setagaya-ku, Tokyo 154-8515, Japan

Vijay Kumar
Institute for Materials Research, Tohoku University, Aoba-ku, Sendai 980-8577, Japan
and Dr. Vijay Kumar Foundation,
45 Bazaar Street, K.K. Nagar (West), Chennai 600 078, India

Kazuo Nakajima and Yoshiyuki Kawazoe
Institute for Materials Research, Tohoku University, Aoba-ku, Sendai 980-8577, Japan
(Received 31 January 2007; revised manuscript received 10 April 2007; published 11 July 2007)

We study the variation in the structural and electronic properties as well as bulk modulus of perovskite-type $R\mathrm{Rh_3B}_x\mathrm{C}_{1-x}$ with R=Sc and Y as a function of the boron concentration. These compounds are realized in the whole range of $0 \leqslant x \leqslant 1$ in cubic structure. We use first-principles projected augmented wave method and the generalized gradient approximation for the exchange-correlation functional within the density-functional theory. Different configurations of boron and carbon atoms for a given x have been studied by considering a $2\times2\times2$ supercell. The atomic structures are fully optimized. The most favorable distribution is found to be the one where like atoms (B or C) are nearest neighbors to each other on the B/C sublattice. However, the energy difference between different configurations is small and at room temperature, B and C atoms are likely to be randomly distributed. The calculated lattice constants are found to be in very good agreement with the experimental results. Our calculations show that the bulk modulus decreases monotonically with increasing boron concentration. We find strong covalent bonding between boron and carbon 2p and Rh 4d orbitals. There is charge transfer to B and C atoms and it is more significant on the B sites. For R=Sc, the cohesive energy is maximum at x=0 and it decreases monotonically with increasing B concentration. However, for R=Y, the highest cohesive energy is obtained for $x \sim 0.25$. For both Sc and Y, the Fermi energy lies in a pseudogap for x=0. Boron doping shifts the Fermi energy in a manner similar to a rigid-band model.

DOI: 10.1103/PhysRevB.76.024105 PACS number(s): 62.20.−x, 61.72.Ji

I. INTRODUCTION

Borides and carbides of transition metals are technologically very important materials due to their high stability and hardness that make them very useful for applications in high-temperature environment, cutting tools, and hard coatings. Moreover, some borocarbides become superconducting at relatively high temperatures such as the Y-Pd-B-C system which has a high T_c of 23 K,[1] and also $\mathrm{MgCNi_3}$ system with T_c of 8 K.[2] Coexistence of magnetism and superconductivity has also been found in some cases.[3,4] It is therefore of considerable interest to understand the electronic properties of such nonoxide perovskites to develop a good understanding of superconductivity also. By changing the relative compositions of metal and nonmetal atoms, it is possible to manipulate the properties of such borocarbides. Here we focus on the $R\mathrm{Rh_3}$-B-C system with R, a rare-earth metal, and study from first-principles calculations the structural, elastic, and electronic properties of $R\mathrm{Rh_3B}_x\mathrm{C}_{1-x}$ compounds with R=Sc and Y. Both Sc and Y are trivalent and one can expect their compounds to have similar properties. Indeed both Sc- and Y-based $R\mathrm{Rh_3}X$, X=B and C compounds, have the same cubic-perovskite-type structure (space group $Pm\bar{3}m$) and form solid solutions in the whole range of B and C concentrations. However, B is trivalent and C is tetravalent. Therefore by changing their relative compositions, the electronic properties are likely to be affected. Furthermore, the strong bonding in these compounds could be optimized by adjusting the relative compositions of B and C as well as the metal elements.

There are only a few studies on these materials. Experiments have been performed in recent years on ternary rare-earth R rhodium borides $R\mathrm{Rh_3B}$ and carbides $R\mathrm{Rh_3C}$.[5–10] Shishido and co-workers[8–10] have studied the dependency of lattice parameters and hardness of $R\mathrm{Rh_3B}_x\mathrm{C}_{1-x}$ system with R=Sc and Y in the range of $0 \leqslant x \leqslant 1$. They have also studied pure rhodium borides and carbides by changing R atoms as well as boron stoichiometry.[11–15] A decrease in the lattice parameter has been obtained with decreasing atomic size of the R element and a corresponding increase in the microhard-

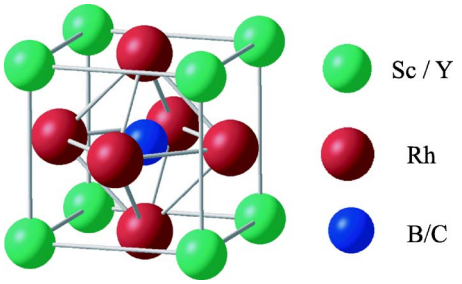

FIG. 1. (Color online) Perovskite cubic unit cell of $R\mathrm{Rh}_3\mathrm{B}_x\mathrm{C}_{1-x}$. R atoms are at the corners while Rh occupies face-center positions. B and C occupy the center of the cube.

ness. For perovskite-type nitride systems such as $M\mathrm{Fe}_3\mathrm{N}$ (M=Ni, Pd, and Pt), ferromagnetic properties have also been studied,[16–18] and the relationship between electronic and elastic properties of these materials has been analyzed by means of first-principles calculations.[19]

Most of the earlier theoretical studies on perovskite-type borocarbide systems[20–25] have been on stoichiometric compounds (x=0 and 1). Recently Sahara *et al.*[26] have performed first-principles calculations on the perovskite-type $\mathrm{ScRh}_3\mathrm{B}_x$ ($0 \leqslant x \leqslant 1$) system in order to understand the variation in the structural properties and bulk modulus as a function of the boron concentration. In these materials, R atoms are at the eight corners of a cube and Rh atoms occupy the six face centers while boron and/or carbon atoms occupy the center of the cube (Fig. 1). Sahara *et al.* found that the maximum bulk modulus is realized surprisingly at x=0.5 contrary to the expectation that vacancies reduce the number of chemical bonds and hence the strength of the compounds. This unexpected behavior has been explained by examining the changes in the atomic and electronic structures of these compounds upon B doping. It is found that B doping enhances the cohesive energy monotonically due to the strong covalent bonding between B $2p$ and Rh $4d$ states. However, at x=0.5 a configuration is achieved where each boron is surrounded by vacancies at the cube centers of the perovskite structure and vice versa. This reduces strain in the structure and the Rh-B bonds become short which lead to a maximum in the bulk modulus. Here in an effort to design strong materials, we have considered the $R\mathrm{Rh}_3\mathrm{B}_x\mathrm{C}_{1-x}$ system in the range of ($0 \leqslant x \leqslant 1$) with R=Sc and Y. This allows the flexibility to change the electron concentration as well as the atomic sizes for optimizing the properties such as the bulk modulus.

In Sec. II we present the calculation procedure. The results are given in Sec. III while Sec. IV summarizes our conclusions.

II. METHOD OF CALCULATION

We follow the calculation method as discussed in Ref. 26 for the case of substoichiometric borides without carbon and use the projected augmented wave (PAW) method[27,28] with the Vienna *ab initio* Simulation Program (VASP).[29–31] Minimization of the free energy over the degrees of freedom of the electronic charge density and ionic positions is performed using the conjugate gradient iterative minimization technique. The exchange-correlation energy is calculated within the generalized gradient approximation (GGA).[32] The cutoff energy for the plane-wave expansion is taken to be 400.0 eV in all the cases. This is large enough to obtain good convergence. A higher cutoff value of 520.0 eV for x=0.5 led to negligible changes in the lattice parameters and about 1% and 0.5% change in the bulk modulus for R=Sc and R=Y, respectively. For the Brillouin-zone (BZ) integrations, we use a mesh of $4\times4\times4$ **k**-points which is also large enough to obtain good convergence. Tests were also made by using $8\times8\times8$ **k**-points and this again led to negligible changes in the lattice parameter as well as small changes in bulk modulus for x=0.5. Therefore all other calculations have been done using $4\times4\times4$ **k**-points. Spin-polarized calculations were also performed to check the occurrence of magnetism due to the presence of transition metals. However, the changes in energy and magnetic moments were found to be negligible.

Furthermore, to treat mixed systems of such borocarbides, although there are methods such as superquasirandom strucutures (SQS) and coherent potential approximation (CPA) which treat solid solutions, we adopted a supercell approach. This is because we would like to analyze the effects of local atomic configurations and displacements from the ideal points on the elastic properties, as our earlier study on $\mathrm{ScRh}_3\mathrm{B}_x$ has shown ordering of boron and vacancy in the case of x=0.5 to be most favorable, and within mean-field theories like CPA such effects may be overlooked. We therefore use a $2\times2\times2$ supercell of the perovskite structure to study substoichiometric compositions. It should be noted that experimentally the compounds have been found to exist in perovskite-type structure in the whole range of boron concentration of $0 \leqslant x \leqslant 1$. We considered different possible distributions of boron and carbon atoms within the supercell for a given concentration of boron to determine energetically the most favorable distribution. Figure 2 shows these configurations for $R\mathrm{Rh}_3\mathrm{B}_x\mathrm{C}_{1-x}$. Here we show only the sublattice sites of boron and carbon atoms, which correspond to the body-center sites of the cubic perovskite cell. Starting from the two limiting cases of x=0 and 1 [Figs. 2(a) and 2(m), respectively] we considered cases with x=0.25 [Figs. 2(b)–2(d)], 0.50 [Figs. 2(e)–2(i)], and 0.75 [Figs. 2(j)–2(l)]. The energies of different configurations as well as the atomic displacements would be useful for further consideration of disorder in these systems.

The bulk modulus B, defined as

$$B = -\frac{Vdp}{dV} = \frac{Vd^2E_{tot}(V)}{dV^2}, \tag{1}$$

with V, the volume of the cell and p, the pressure, is estimated with high accuracy using the Murnaghan equation of state,[33]

$$E_{tot}(V) = \frac{B_0V}{B_0'(B_0'-1)}\left[B_0'\left(1-\frac{V_0}{V}\right)+\left(\frac{V_0}{V}\right)^{B_0'}-1\right]+E_{tot}(V_0). \tag{2}$$

Here $E_{tot}(V)$ is the total energy of the system at volume V, and B_0 and B_0' are the bulk modulus and its pressure deriva-

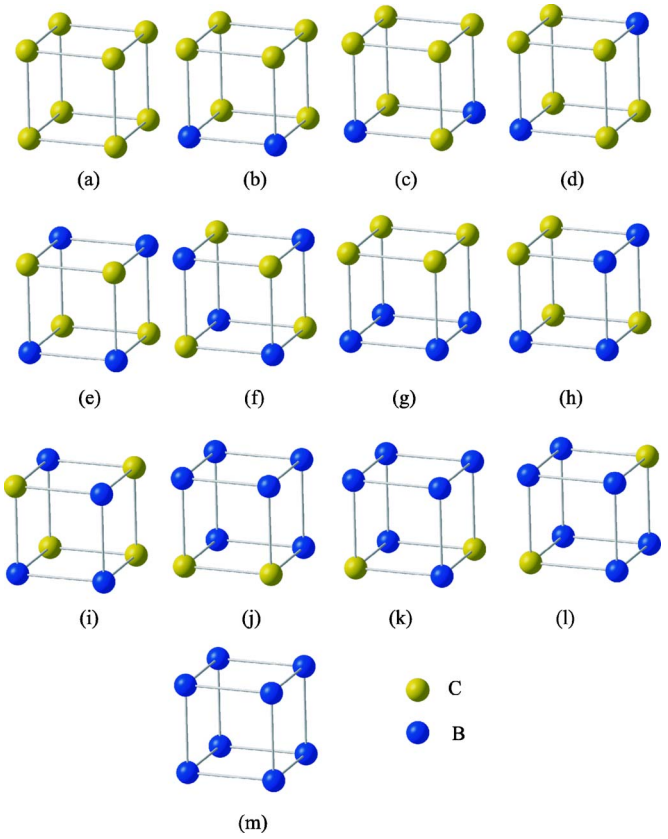

FIG. 2. (Color online) Different configurations of boron and carbon atoms in a $2\times2\times2$ supercell of $ScRh_3B_xC_{1-x}$ for (a) $x=0$, (b)–(d) $x=0.25$, (e)–(i) $x=0.5$, (j)–(l) $x=0.75$, and (m) $x=1$ as used in the present calculations. Only the sublattice sites that nonmetal atoms occupy and which correspond to the body-center sites of the cubic perovskite cells, are shown. Blue (yellow) balls correspond to B (C).

tive at the equilibrium volume V_0, respectively. We calculated $E_{tot}(V)$ for 12 different volumes using cubic perovskite cells and the values were fitted with Eq. (2). Further the solid-solution-like distribution of B and C atoms can create strain in the structure. As the experiments suggest cubic structure, we performed calculations using a cubic structure as the initial condition. For atomic relaxations, two approaches have been used: (i) in which cubic structure is kept for all boron concentrations with atoms placed as in perovskite structure, and (ii) in which atomic positions are optimized allowing changes in the lattice parameters to check the stability of the cubic cell, especially for the low symmetric cases.

III. RESULTS AND DISCUSSION

The results of the optimized lattice parameters along with the initial structural parameters are given in Tables I and II for $ScRh_3B_xC_{1-x}$ and $YRh_3B_xC_{1-x}$, respectively. It can be noted that the changes in the lattice parameters obtained from the optimization of the stresses and from the Murnaghan equation of state, assuming cubic structure in all cases, are small. For the substoichiometric compositions, the lowest energy (highest stability) configuration in the case of boron concentration of $x=0.25$, 0.5, and 0.75 are shown in Figs. 2(b), 2(g), and 2(j), respectively. These are similar for $R=$Sc and Y. Our results show that like atoms, namely B or C, tend to segregate in these borocarbides. This behavior is different from the case of vacancies in borides where vacancies and B atoms have a tendency to be nearest neighbor on the boron sublattice. However, in the present case the energy difference among the different configurations of C and B atoms for a given substoichiometric concentration x is very small (see discussion later). Therefore at room temperature one can expect random distribution of B and C atoms on the B/C sublattice. For $x=0$ [Fig. 2(a)] and $x=1$ [Fig. 2(m)], the structure remains cubic while for $x=0.25$, 0.5, and 0.75 there are noncubic distortions in the lowest energy optimized structures, although generally these are negligibly small (about 0.1%). In experiments under conditions of normal temperature and pressure, these systems are likely to have a distribution of boron and carbon atoms which is not perfectly ordered. A random distribution would lead to a cubic structure on an average as observed. We estimated the mean cubic lattice parameter in the cases of noncubic distortions and the calculated values agree very closely with the values obtained from the Murnaghan equation of state assuming cubic structure.

Since experimental results show cubic structure over the whole composition of boron,[6,7] we have shown in Fig. 3 the relationship between the calculated equilibrium lattice constant for cubic structures and boron concentration x. It shows that the lattice constant decreases monotonically as x increases and that the calculated values are in very good agreement (within ~2%) with the experimental results. There is a slight overestimation of the lattice constant for the whole concentration range which is often a feature of GGA. The lattice constant is larger for the case of $R=$Y as Y atom is bigger than Sc. The calculated equilibrium volume of $RRh_3B_xC_{1-x}$ nearly obeys Vegard's law, $V_{eq}(x)=xV_{eq}^{RRh_3B}+(1-x)V_{eq}^{RRh_3C}$. In the figure, the solid lines correspond to Vegard's law prediction, which was obtained by the equilibrium lattice constants for $x=0$ and 1. Also the deviations in the experimental values from Vegard's law are quite small.

The cohesive energy for different x and for different distributions of boron and carbon atoms is shown in Fig. 4. Here, cohesive energy is defined as energy required to form separated atoms from the solid. The values correspond to the optimized structures allowing changes in the lattice parameters only, the energy difference between the cases of assuming cubic unit cells and the optimized cells being very small. Also the variation in the values of the cohesive energy for different configurations corresponding to a given concentration x is very small as shown for $x=0.25$, 0.5, and 0.75. For example, the energy differences between the most stable and the second most stable configurations are 2.1×10^{-2}, 2.9×10^{-2}, 1.6×10^{-2}, 2.6×10^{-3}, 1.1×10^{-2}, and 1.5×10^{-3} eV per supercell for $ScRh_3B_{0.25}C_{0.75}$, $ScRh_3B_{0.5}C_{0.5}$, $ScRh_3B_{0.75}C_{0.25}$, $YRh_3B_{0.25}C_{0.75}$, $YRh_3B_{0.5}C_{0.5}$, and $YRh_3B_{0.75}C_{0.25}$, respectively. In the case of $R=$Y, the cohesive energy becomes slightly lower for low concentration of boron. It increases for higher concentrations and then decreases again with increasing x. The cohesive energy for R

TABLE I. Initial and optimized structural parameters in Å for the supercell, and the bulk modulus for $ScRh_3B_xC_{1-x}$. Indexing of the configuration is defined in Fig. 2. For the final structure, results are given for the two methods used for the optimization of the unit cell. One in which all the lattice parameters are optimized and the other in which the cubic structure is kept for all concentrations. Bulk modulus is given for the cubic structure.

	Initial structural parameter	Final structural parameter					
		Optimized cell parameter					
x	Cubic structure a axis	a axis	b axis	c axis	Mean lattice parameter	Cubic structure a axis	Bulk modulus (GPa)
0.000 (a)	8.200	8.203	8.203	8.203	8.203	8.203	217
0.250 (b)	8.210	8.210	8.214	8.214	8.213	8.213	213
0.250 (c)	8.210	8.212	8.214	8.214	8.213	8.213	213
0.250 (d)	8.210	8.214	8.214	8.214	8.214	8.213	212
0.500 (e)	8.220	8.223	8.232	8.232	8.229	8.225	208
0.500 (f)	8.220	8.228	8.228	8.228	8.228	8.225	208
0.500 (g)	8.220	8.234	8.223	8.223	8.227	8.224	208
0.500 (h)	8.220	8.227	8.226	8.226	8.226	8.224	208
0.500 (i)	8.220	8.227	8.224	8.224	8.225	8.225	208
0.750 (j)	8.230	8.234	8.237	8.237	8.236	8.236	203
0.750 (k)	8.230	8.239	8.240	8.240	8.240	8.236	202
0.750 (l)	8.230	8.237	8.237	8.237	8.237	8.237	202
1.000 (m)	8.250	8.251	8.251	8.251	8.251	8.249	198

=Sc is higher for x less than ≈ 0.7 compared with the values for R=Y. For larger x there is a crossover and the cohesive energy for R=Y becomes higher until x=1. This behavior can be understood considering the change in the lattice parameter. The lattice parameter for R=Y is larger compared with R=Sc and therefore a bigger size atom, B as compared to C, becomes more favorable and leads to higher cohesive energy for R=Y, x=1. On the other hand, in the region close to x=0, the lattice parameter has a lower value and therefore a smaller size atom, Sc, provides better bonding and it results in a higher value of the cohesive energy for $ScRh_3C$. For the intermediate values of x, a crossover occurs.

Figure 5 shows the variation in the bulk modulus with boron concentration. Again we have shown the results for all the calculated configurations for each x. The small variation in the values for different configurations reflects the behavior

TABLE II. Same as in Table I but for $YRh_3B_xC_{1-x}$.

	Initial structural parameter	Final structural parameter					
		Optimized cell parameter					
x	Cubic structure a axis	a axis	b axis	c axis	Mean lattice parameter	Cubic structure a axis	Bulk modulus (GPa)
0.000 (a)	8.400	8.376	8.376	8.376	8.376	8.377	198
0.250 (b)	8.400	8.388	8.390	8.390	8.389	8.390	193
0.250 (c)	8.400	8.387	8.390	8.390	8.389	8.391	193
0.250 (d)	8.400	8.388	8.388	8.388	8.388	8.390	193
0.500 (e)	8.400	8.396	8.407	8.407	8.403	8.404	189
0.500 (f)	8.400	8.402	8.402	8.402	8.402	8.404	189
0.500 (g)	8.400	8.404	8.404	8.404	8.404	8.404	189
0.500 (h)	8.400	8.404	8.401	8.401	8.402	8.404	189
0.500 (i)	8.400	8.406	8.404	8.404	8.405	8.404	189
0.750 (j)	8.400	8.414	8.418	8.418	8.417	8.417	186
0.750 (k)	8.400	8.417	8.419	8.419	8.418	8.417	186
0.750 (l)	8.400	8.417	8.417	8.417	8.417	8.417	186
1.000 (m)	8.400	8.432	8.432	8.432	8.432	8.431	183

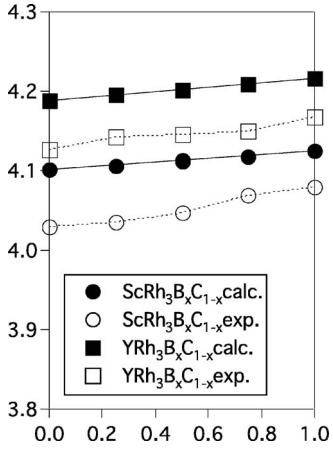

FIG. 3. Relationship between cubic lattice constant and boron concentration. Solid circles and squares correspond to the present results while the unfilled circles and squares are the experimental data from Refs. 8 and 11. The solid lines show the Vegard's law prediction.

found for the cohesive energy. The bulk modulus is higher for R=Sc for the whole range of x. The bulk modulus decreases with increasing x for both R=Sc and Y. This behavior agrees with the general tendency of a decrease in bulk modulus with increasing lattice parameter (see Fig. 3). The bulk modulus in the case of R=Y is lower than the value for R=Sc because it has larger lattice constant compared with the case of Sc doping (Tables I and II).

We further studied the variation in the electronic structure of $R\mathrm{Rh_3C}$ as well as the changes in the local atomic structure

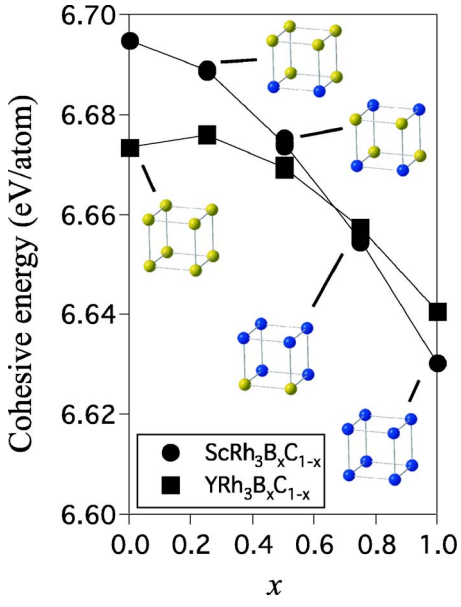

FIG. 4. (Color online) Relationship between the cohesive energy per atom and boron concentration x. The values are given for cubic unit cells but the deviation from values obtained from full atomic relaxations is quite small. Different points for a given x correspond to the different distributions of boron and carbon atoms (see Fig. 2). However, the variation in values for a given x is small. The insets show the lowest energy configurations of B and C atoms in the supercell.

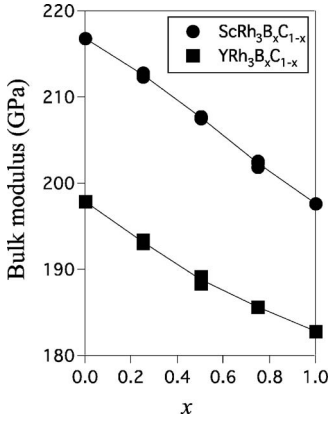

FIG. 5. Relationship between the bulk modulus and boron concentration. The results for all the configurations calculated in the present study are given.

due to the doping of boron. Figure 6 shows the total and the site-projected density of states (DOS) along with the angular momentum decomposition for (a) $\mathrm{ScRh_3C}$, (b) $\mathrm{ScRh_3B_{0.5}C_{0.5}}$, (c) $\mathrm{ScRh_3B}$, (d) $\mathrm{YRh_3C}$, (e) $\mathrm{YRh_3B_{0.5}C_{0.5}}$, and (f) $\mathrm{YRh_3B}$ as examples. In the case of x=0.5, the results are shown for the energetically most stable configuration [see Fig. 2(g)]. The total and the partial DOS for $R\mathrm{Rh_3C}$ in Figs. 6(a) and 6(b) show that the 4s and 4p (5s and 5p) orbitals of Sc (Y) have significant charge transfer to Rh. This will be further shown clearly from the discussion of the charge-density distribution later. The 3d (4d) orbitals of Sc (Y) hybridize with those of Rh but most of the occupied states are the Rh 4d states. Therefore the bonding between Sc (Y) and Rh is ionic with some covalent character. These general features of R and Rh bonding also exist in other cases when boron is doped. The Fermi energy lies in a pseudogap for x=0. Therefore the carbides with zero boron content should exhibit extra stability. Doping of B shifts the Fermi energy due to the depletion of electrons in a rigid-band-like manner near the Fermi energy where the main features of the d electronic states remain very similar. Significant metallic contribution of Rh 4d states can also be seen for all the cases. There is a peak at the bottom of the total DOS and it can be seen in the partial DOS of boron or carbon for the cases of x=1 or 0 in Figs. 6. This is derived from boron or carbon 2s orbital and it has little hybridization with the Rh or Sc orbitals. However, the 2p orbitals of boron or carbon hybridize strongly with the 4d orbitals of Rh and there are bonding states (at around ~−5 to −7 eV) near the bottom of the d band. The antibonding hybridized states lie above the Fermi level and these nearly overlap with the Rh 4d states. The weak hybridization with Y 4d states can be seen in Figs. 6(d)–6(f) where Y 4d states are well separated from the Rh 4d states.

In order to further check the bonding character as well as charge transfers, we have shown in Figs. 7(a)–7(c) the electronic charge density for x=0, 0.5, and 1, respectively, in the (011) plane which passes through Sc, Rh, and boron or carbon ions. These results clearly show covalent bonding nature between boron or carbon and Rh atoms as described above and little charge around Sc ions. In the case of R=Y, we also

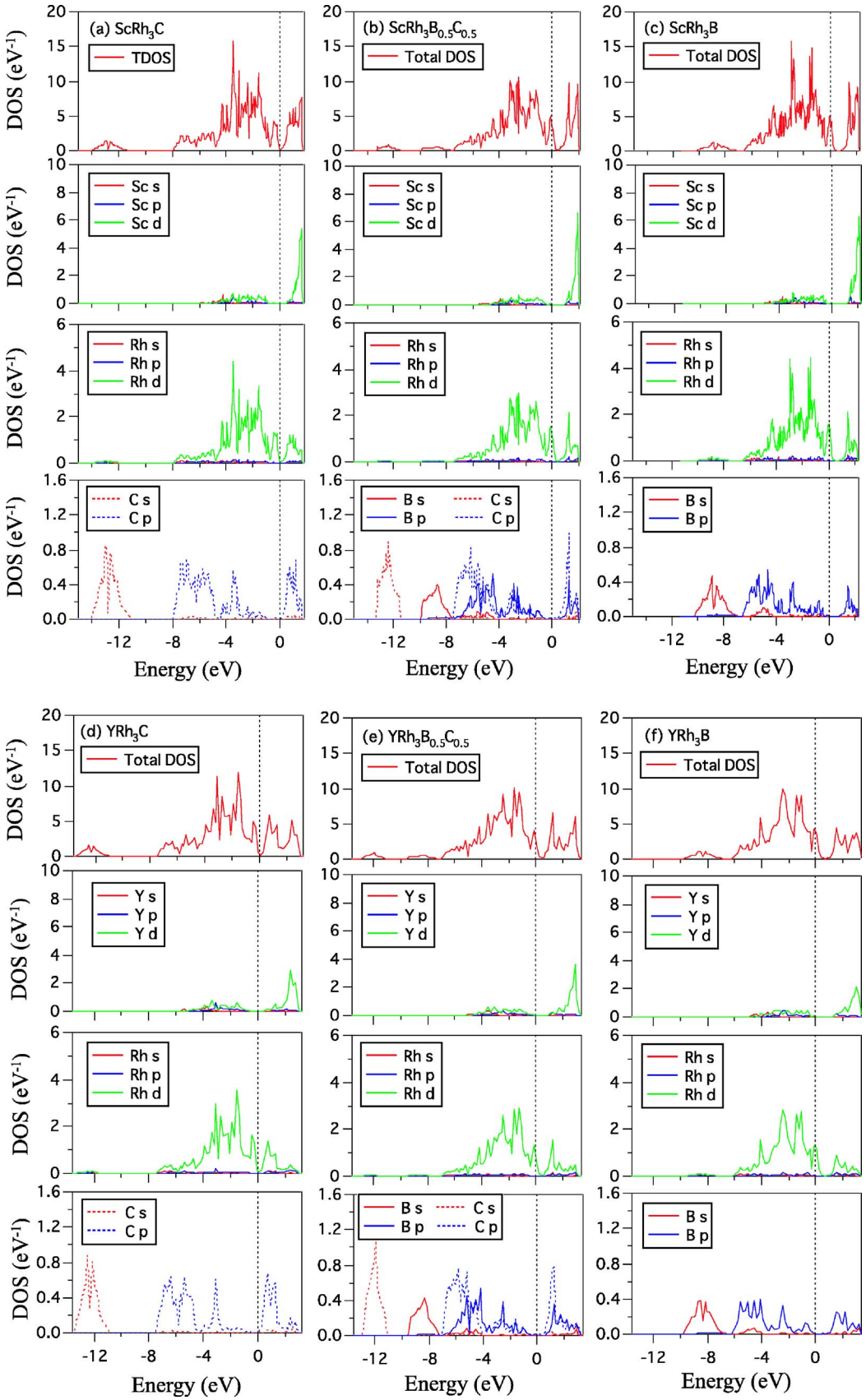

FIG. 6. (Color online) Total density of states and the site-projected partial density of states for (a) $ScRh_3C$, (b) $ScRh_3B_{0.5}C_{0.5}$, (c) $ScRh_3B$, (d) YRh_3C, (e) $YRh_3B_{0.5}C_{0.5}$, and (f) YRh_3B. Fermi energy lies at the zero of energy. Angular momentum decomposed partial DOS are also shown.

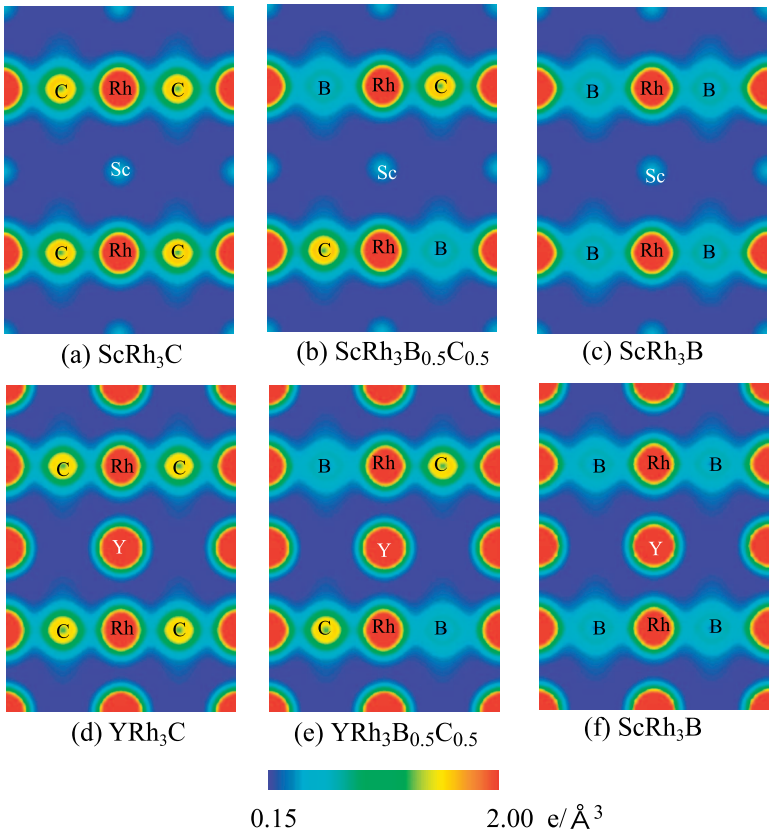

FIG. 7. (Color) Electronic charge density plots in (011) plane passing through the cube center of a cell for (a) $ScRh_3C$, (b) $ScRh_3B_{0.5}C_{0.5}$, (c) $ScRh_3B$, (d) YRh_3C, (e) $YRh_3B_{0.5}C_{0.5}$, and (f) YRh_3B. The low electronic charge density around Sc ions is clearly seen. The highest charge density appears close to the core of the Rh ions and has the value of about 4.6 electron/Å^3. However, in the figure we have used the values up to 2.0 electron/Å^3 to clarify the covalent bonding between Rh and B/C.

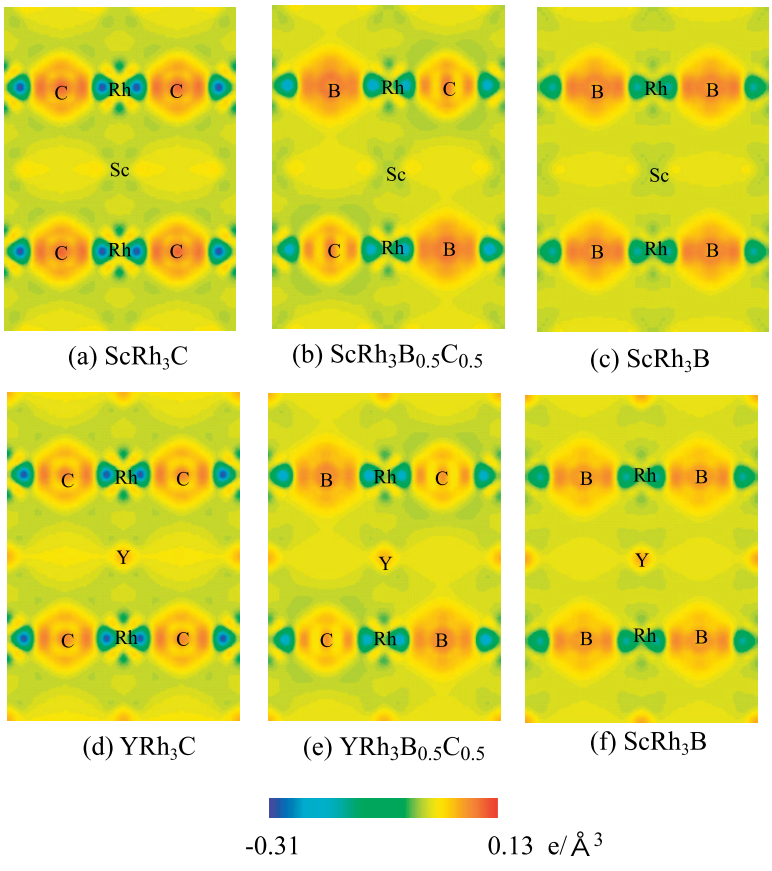

FIG. 8. (Color) Plot of the electronic charge density difference between the borocarbides and RRh_3 plus carbon or boron atoms at the respective positions in (011) plane for (a) $ScRh_3C$, (b) $ScRh_3B_{0.5}C_{0.5}$, (c) $ScRh_3B$, (d) YRh_3C, (e) $YRh_3B_{0.5}C_{0.5}$, and (f) YRh_3B. Depletion of charge around Rh ions and buildup of charge around C and B ions can be seen.

TABLE III. Lattice constant of the supercell, Rh-B and Rh-C bond lengths, and the corresponding number of bonds for $ScRh_3B_xC_{1-x}$. Displacement of R atom from the ideal position and the corresponding number of atoms (n) are also shown. The indexing of the configuration in the column of x is defined in Fig. 2.

x	Lattice constant (Å)	Rh-B (n) (Å)	Rh-C (n) (Å)	Displacement of Sc from the ideal position (Å)
0.000 (a)	8.203		2.051 (48)	0.000 (8)
0.250 (b)	8.213	2.052 (4)	2.025 (8)	0.040 (8)
		2.082 (8)	2.050 (8)	
			2.052 (12)	
			2.057 (8)	
0.500 (e)	8.229	2.056 (8)	2.034 (16)	0.000 (8)
		2.082 (16)	2.056 (8)	
0.750 (j)	8.236	2.055 (8)	2.032 (8)	0.036 (8)
		2.058 (12)	2.058 (4)	
		2.063 (8)		
		2.087 (8)		
1.000 (m)	8.251	2.063 (48)		0.000 (8)

TABLE IV. Same as in Table III but for $YRh_3B_xC_{1-x}$.

x	Lattice constant (Å)	Rh-B (n) (Å)	Rh-C (n) (Å)	Displacement of Y from the ideal position (Å)
0.000 (a)	8.376		2.094 (48)	0.000 (8)
0.250 (b)	8.389	2.097 (4)	2.058 (8)	0.024 (8)
		2.137 (8)	2.088 (8)	
			2.097 (12)	
			2.107 (8)	
0.500 (e)	8.403	2.099 (8)	2.071 (16)	0.000 (8)
		2.133 (16)	2.099 (8)	
0.750 (j)	8.417	2.099 (8)	2.068 (8)	0.024 (8)
		2.104 (12)	2.104 (4)	
		2.110 (8)		
		2.141 (8)		
1.000 (m)	8.431	2.108 (48)		0.000 (8)

included the semicore $4p$ states as valence states and therefore in Figs. 7(d)–7(f) there is high electronic charge density around Y ions. However, there is little charge between Y and Rh ions. Furthermore, the electronic charge density around carbon ions is higher than in the case of boron. In order to see the charge transfer we plotted the difference in the electronic charge density between borides or carbides and the sum of the hypothetical RRh_3 system and the B/C atoms on the same positions as in the perovskites. The results are shown in Fig. 8. There is depletion of charge from the vicinity of Rh and accumulation of charge around C and B ions. The accumulation is more around B ions. For R=Sc, very little change occurs around Sc ions due to the B/C doping, but for R=Y, there is a small increase in the electronic charge density.

Finally, the effects of doping on the atomic structure are obtained from the relaxation of Rh ions within the supercell when boron is doped. From Fig. 3, we note a continuous increase in the lattice constant with boron doping (see also Tables III and IV). Doping of boron atoms displaces the neighboring Rh ions outwards from their lattice position, but the displacements are small. As shown in Tables III and IV, there is an increase in the averaged Rh-B bond length with an increase in the boron concentration and it leads to the weakening of these covalent bonds and hence a decrease in the bulk modulus. The interatomic distances between Rh-B and Rh-C are slightly different and it could be a reason for the segregation tendency of B and C in order to minimize strain.

IV. SUMMARY

In summary we have performed first-principles calculations on $RRh_3B_xC_{1-x}$ with R=Sc and Y in the perovskite structure to obtain the equilibrium lattice constants and the bulk modulus. The calculated equilibrium lattice constants are found to be in very good agreement with the experimental results. The cohesive energy is higher for YRh_3B as compared to $ScRh_3B$ while the reverse happens for the pure carbides. In the intermediate range of B concentration, there is a crossover. Boron doping leads to a continuous decrease in the bulk modulus. The origin of these properties has been explained in terms of the changes in the covalent and ionic bonding characters.

ACKNOWLEDGMENTS

The authors are grateful to the staff of the Center for Computational Materials Science of IMR, Tohoku University, and the Center for Computational Science and Systems of the Japan Atomic Energy Agency (JAEA) for their continuous support of the computing system. This research has been partially carried out by using ITBL (IT Based Laboratory) environment. The authors would like to thank to the Sumitomo Foundation for financial support. V.K. thankfully acknowledges the kind hospitality at the IMR and the International Frontier Center for Advanced Materials (IFCAM) of IMR.

*Electronic address: sahara@imr.edu

[1] R. J. Cava and H. Takagi, B. Batlogg, H. W. Zandbergen, J. J. Krajewski, W. F. Peck, Jr., R. B. van Dover, R. J. Felder, T. Siegrist, K. Mizuhashi, J. O. Lee, H. Eisaki, S. A. Carter, and S. uchida, Nature (London) **367**, 146 (1994).

[2] T. He, Q. Huang, A. P. Ramirez, Y. Wang, K. A. Regan, N. Rogado, M. A. Hayward, M. K. Haas, J. S. Slusky, K. Inumara, H. W. Zandbergen, N. P. Ong, and R. J. Cava, Nature (London) **411**, 54 (2001).

[3] T. Watanabe, M. Nohara, T. Hanaguri, and H. Takagi, Phys. Rev. Lett. **92**, 147002 (2004).

[4] L. N. Bulaevskii, M. Hruška, and M. P. Maley, Phys. Rev. Lett. **95**, 207002 (2005).

[5] P. Rogl and L. Delong, J. Less-Common Met. **91**, 97 (1983).

[6] T. Shishido, J. Ye, T. Sasaki, R. Note, K. Obara, T. Takahashi, T. Matsumoto, and T. Fukuda, J. Solid State Chem. **133**, 82 (1997).

[7] T. Shishido, J. Ye, S. Okada, K. Kudou, T. Sasaki, S. Ishida, T. Naka, M. Oku, I. Higashi, H. Kishi, H. Horiuchi, and T. Fukuda, J. Alloys Compd. **280**, 65 (1998).

[8] T. Shishido, J. Ye, S. Okada, K. Kudou, K. Iizumi, M. Oku, Y. Ishizawa, T. Amano, S. Kohiki, Y. Kawazoe, and K. Nakajima, J. Alloys Compd. **354**, 198 (2003).

[9] T. Shishido, J. Ye, K. Kudou, S. Okada, K. Iizumi, M. Oku, Y. Ishizawa, A. Yoshikawa, M. Tanaka, S. Oishi, N. Kamegashira, S. Kohiki, Y. Kawazoe, and K. Nakajima, Jpn. J. Appl. Phys., Part 1 **42**, 5213 (2003).

[10] T. Shishido, J. Ye, K. Kudou, S. Okada, K. Obara, T. Sugawara, M. Oku, K. Wagatsuma, H. Horiuchi, and T. Fukuda, J. Alloys Compd. **291**, 52 (1999).

[11] T. Shishido, J. Ye, S. Okada, K. Kudou, T. Sasaki, S. Isida, T. Naka, M. Oku, I. Higashi, H. Kishi, H. Horiuchi, and T. Fukuda, J. Alloys Compd. **309**, 107 (2000).

[12] T. Shishido, K. Kudou, S. Okada, J. Ye, A. Yoshikawa, T. Sasaki, M. Oku, H. Horiuchi, I. Higashi, S. Kohiki, Y. Kawazoe, and K. Nakajima, Jpn. J. Appl. Phys., Part 1 **40**, 6037 (2001).

[13] T. Shishido, J. Ye, S. Okada, K. Kudou, M. Oku, K. Obara, T. Sugawara, A. Yoshikawa, Y. Ishizawa, M. Ogawa, K. Iizumi, I. Higashi, T. Amano, S. Kohiki, Y. Kawazoe, and K. Nakajima, Jpn. J. Appl. Phys., Part 1 **41**, 3031 (2002).

[14] T. Shishido, Y. Ishizawa, J. Ye, S. Okada, K. Kudou, K. Iizumi, M. Oku, M. Tanaka, A. Yoshikawa, A. Nomura, T. Sugawara, S. Tozawa, K. Obara, S. Oishi, N. Kamegashira, T. Amano, R. Sahara, V. Kumar, H. Horiuchi, S. Kohiki, Y. Kawazoe, and K. Nakajima, J. Alloys Compd. **408–412**, 375 (2006).

[15] T. Shishido, J. Ye, S. Okada, K. Kudou, K. Iizumi, M. Oku, Y. Ishizawa, R. Sahara, V. Kumar, A. Yoshikawa, M. Tanaka, H. Horiuchi, A. Nomura, T. Sugawara, K. Obara, T. Amano, S. Kohiki, Y. Kawazoe, and K. Nakajima, J. Alloys Compd. **408–412**, 379 (2006).

[16] H. H. Stadelmaier and A. C. Franker, Trans. Metall. Soc. AIME **218**, 571 (1960).

[17] K. K. Shih, M. E. Re, T. Takamori, and D. B. Dove, J. Appl. Phys. **71**, 5539 (1992).

[18] K. K. Shih and J. Karasinski, J. Appl. Phys. **73**, 8377 (1993).

[19] D. Music and J. M. Schneider, Appl. Phys. Lett. **88**, 031914 (2006).

[20] R. E. Schaak, M. Avdeev, W. L. Lee, G. Lawes, H. W. Zandbergen, J. D. Jorgensen, N. P. Ong, A. P. Ramirez, and R. J. Cava, J. Solid State Chem. **177**, 1244 (2004).

[21] P. Ravindran, S. Sankaralingam, and R. Asokamani, Phys. Rev. B **52**, 12921 (1995).

[22] M. Oku, T. Shishido, T. Shinohara, T. Fukuda, Q. Sun, Y. Kawazoe, and K. Wagatsuma, J. Alloys Compd. **339**, 317 (2002).

[23] M. Oku, T. Shishido, K. Wagatsuma, Q. Sun, and Y. Kawazoe, J. Alloys Compd. **349**, 206 (2002).

[24] D. Music, Z. Sun, and J. M. Schneider, Phys. Rev. B **71**, 052104 (2005).

[25] R. Sahara, T. Shishido, A. Nomura, K. Kudou, S. Okada, V. Kumar, K. Nakajima, and Y. Kawazoe, Comput. Mater. Sci. **36**, 12 (2006).

[26] R. Sahara, T. Shishido, A. Nomura, K. Kudou, S. Okada, V. Kumar, K. Nakajima, and Y. Kawazoe, Phys. Rev. B **73**, 184102 (2006).

[27] G. Kresse and D. Joubert, Phys. Rev. B **59**, 1758 (1999).

[28] P. E. Blöchl, Phys. Rev. B **50**, 17953 (1994).

[29] G. Kresse and J. Hafner, Phys. Rev. B **47**, R558 (1993); **49**, 14251 (1994).

[30] G. Kresse and J. Fürthmuller, Phys. Rev. B **54**, 11169 (1996).

[31] G. Kresse and J. Hafner, J. Phys.: Condens. Matter **6**, 8345 (1994).

[32] J. P. Perdew, in *Electronic Structure of Solids '91*, edited by P. Ziesche and H. Eschrig (Akademie Verlag, Berlin, 1991).

[33] F. D. Murnaghan, Proc. Natl. Acad. Sci. U.S.A. **30**, 244 (1944).